# Near-Field Optical Mapping of Exciton Wave Functions in a GaAs Quantum Dot

K. Matsuda,[1,2,*] T. Saiki,[1,3] S. Nomura,[4,5] M. Mihara,[5] Y. Aoyagi,[5,6] S. Nair,[7] and T. Takagahara[8]

[1]*Kanagawa Academy of Science and Technology, 3-2-1 Sakado, Takatsu, Kawasaki, Japan*
[2]*Nanostructure and Material Property, PRESTO, Japan Science and Technology Agency (JST), 4-1-8 Honcho Kawaguchi, Saitama, Japan*
[3]*Department of Electronics and Electrical Engineering, Keio University, 3-14-1 Hiyoshi, Kohoku, Yokohama, Kanagawa, Japan*
[4]*Institute of Physics, University of Tsukuba, 1-1-1 Tsukuba, Ibaraki, Japan*
[5]*Semiconductors Laboratory, The Institute of Physical and Chemical Research (RIKEN), 2-1 Hirosawa, Wako, Saitama, Japan*
[6]*Interdisciplinary Graduate School of Science and Engineering, Tokyo Institute of Technology, 4259 Nagatsuda, Midori, Yokohama, Japan*
[7]*Center for Advanced Nanotechnology, University of Toronto, 170 College Street, Toronto, Ontario M5S 3E3, Canada*
[8]*Department of Electronics and Information Science, Kyoto Institute of Technology, Matsugasaki, Sakyo, Kyoto, Japan*

(Received 31 May 2003; published 20 October 2003)

Near-field photoluminescence imaging spectroscopy of naturally occurring GaAs quantum dots (QDs) is presented. We successfully mapped out center-of -mass wave functions of an exciton confined in a GaAs QD in real space due to the enhancement of spatial resolution up to 30 nm. As a consequence, we discovered that the spatial profile of the exciton emission, which reflects the shape of a monolayer-high island, differs from that of biexciton emission, due to different distributions of the polarization field for the exciton and biexciton recombinations. This novel technique can be extensively applied to wave function engineering in the design and the fabrication of quantum devices.

DOI: 10.1103/PhysRevLett.91.177401 PACS numbers: 78.55.Cr, 71.35.–y, 78.67.Hc

Quantum two-level systems with long coherence times are candidates for the basic component of quantum computing and quantum information processing devices [1–3]. The exciton in a quantum dot (QD) is an ideal two-level system due to the QD's discrete electronic density of states [4–8]. The exciton in a naturally formed QD [a monolayer-high island formed in a narrow quantum well (QW) [4,5,9–14]], which exhibits long duration of coherence at low temperature [11] and a large dipole moment [12], provides us with light-controllable quantum bits. These characteristics of an exciton quantum system in a QD have been measured by making full use of precise optical spectroscopy in both the frequency and time domains with a subwavelength spatial resolution to address a single QD [4–13]. However, to improve such parameters as coherence time and dipole moment, accurate information on the wave function for individual QDs is of great importance. In addition, in the study of coupled-QD systems as multiquantum bits, in which it is difficult to predict the exact wave function within theoretical frameworks, an optical spectroscopic technique for probing the wave function itself should be developed.

Near-field scanning optical microscopes (NSOM) have been utilized to study the local density of states (LDOS) of elementary excitation by offering a subwavelength spatial resolution. Chicanne *et al.* reported an experimental observation of optical LDOS for an optical corral structure with a "forbidden light" NSOM [15,16]. In analogy to this, in the study of semiconductor quantum-confined structures, NSOM with spectral selectivity can be also applied to image the optical LDOS (distribution of optical dipole) for single eigenstates [13]. Theoretical studies predict that the optical LDOS is directly connected to the (center-of-mass) wave functions of electron-hole pair (exciton) via the calculation of transition rate as a function of probe position [17,18]. Such a possibility, however, has not been investigated while NSOM contribute to the spectroscopy of a single quantum object by isolating individual components with a spatial resolution of 100–200 nm [19–22]. Enhancement of spatial resolution up to 10–30 nm, which is smaller than the typical size of quantum constituents, is of critical importance to precisely map out the wave function of a confined exciton.

In this Letter, we report near-field photoluminescence (PL) imaging spectroscopy of a naturally occurring GaAs QD formed in a narrow QW. Because of the enhancement of spatial resolution up to 30 nm, we directly observe that the exciton and biexciton are confined in elongated monolayer-high islands along $[\bar{1}10]$ crystal axis through the exciton and biexciton PL images. The clear difference in the spatial profile between exciton and biexciton emission is well accounted for by the theoretically calculated polarization field for the exciton and biexciton recombination. The theoretical support and experimental results indicate that the near-field optical probe with high spatial resolution relative to the size of the QD enables a real-space mapping of the center-of-mass wave function of an exciton confined in the QD.

For the target of the imaging spectroscopy, we prepared a 5 nm thick GaAs QW, sandwiched between layers of AlAs and $Al_{0.3}Ga_{0.7}As$ grown by molecular-beam epitaxy shown in Fig. 1. Two-minute interruptions of the

  

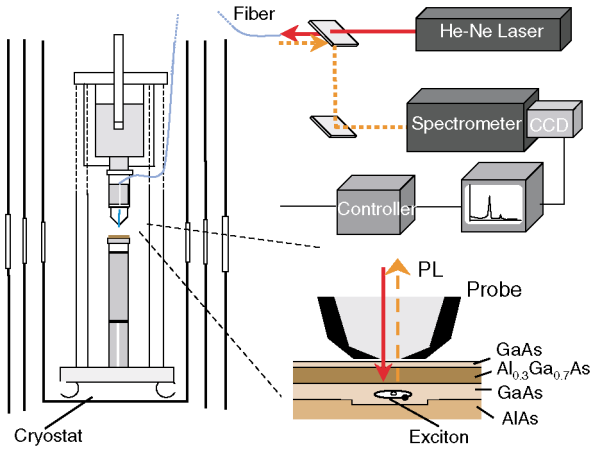


FIG. 1 (color). Schematic of low temperature near-field scanning optical microscope and experimental setup of near-field photoluminescence (PL) measurement. Sample structures of naturally occurring quantum dot (QD) in a narrow quantum well and the near-field probe are shown.

growth process at both interfaces promote the formation of natural QDs [4,5,9–14]. The narrow GaAs QW layer was covered with a thin barrier of a 15 nm $Al_{0.3}Ga_{0.7}As$ and a cap layer of 5 nm GaAs. The thin barrier and cap layers allow the near-field tip to be close enough to the emission source (QD) to achieve a spatial resolution as high as 30 nm [23].

The critical element in the high-resolution NSOM measurement was an optical fiber probe, which was fabricated by chemical etching with a hydrofluoric acid solution [22,23]. The tapered structure was optimized by taking account of trade-off between optical throughput and spatial resolution. A small clear aperture was prepared by pounding the probe apex against the sample surface under shear-force feedback control. The aperture diameter (20 nm) was estimated from scanning electron micrographs, taken after conducting near-field imaging measurements at cryogenic temperature. A spatial resolution as high as 30 nm was demonstrated by low temperature PL imaging of self-assembled InAs QDs with a 30 nm aperture probe [23]. The sample of GaAs QDs was excited with He-Ne laser light ($\lambda = 633$ nm) through the aperture and the resultant PL signal was collected via the same aperture to prevent a reduction of the spatial resolution due to carrier diffusion as shown in Fig. 1 [24]. Near-field PL spectra were measured, for example, at 11 nm steps across a $210 \times 210$ nm$^2$ area and two-dimensional images were constructed from a series of PL spectra.

We show in Fig. 2(a) near-field PL spectra of a single QD at 9 K at excitation powers ranging from 0.17 to 3.8 $\mu$W. The power indicates the laser intensity coupled to the fiber probe, not ejected from the aperture. A sharp emission line (denoted by X) at 1.6088 eV is observed. With an increase in excitation power, another emission line appears at 1.6057 eV (denoted by XX). In order to clarify the origin of these emissions, we show the excitation power dependence of PL intensities in Fig. 2(b) [25]. The red (blue) dotted line in Fig. 2(b) corresponds to the gradient associated with linear (quadratic) power dependence. The X line can be identified as an emission from a single-exciton state by its linear increase in emission intensity and its saturation behavior. The quadratic dependence of the XX emission with excitation power indicates that XX is an emission from a biexciton state. This identification of the XX line is also supported by the correlation energy of 3.1 meV, which agrees well with the values reported previously [9,14]. Figures 2(c)–2(e) show

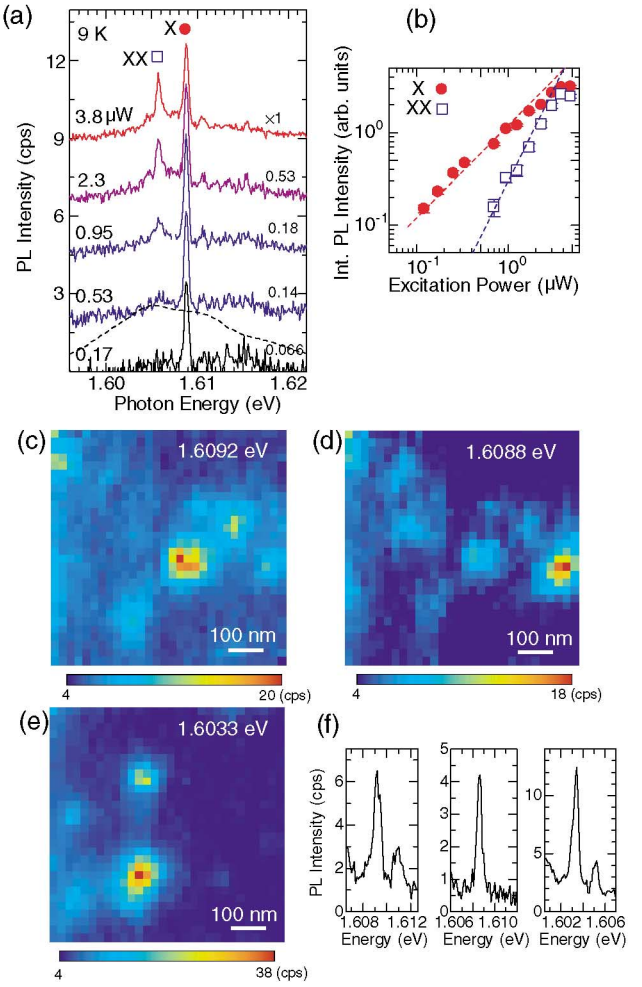


FIG. 2 (color). Near-field PL spectra of a single QD (solid lines) and far-field PL spectrum (dotted line) at 9 K (a). The PL peaks at 1.6088 and 1.6057 eV are denoted by X and XX. Excitation power dependence of integrated PL intensities of the X and the XX lines (b). The red (blue) dotted line corresponds to the gradient associated with linear (quadratic) power dependence. Near-field PL images obtained by mapping the intensity of the X lines in a same scanning area ($1000 \times 1000$ nm$^2$) (c)–(e). The PL spectra for generating each image are indicated (f). The QDs in (c) and (d) are in one-monolayer thinner regions and the one in (e) is in a one-monolayer thicker region.

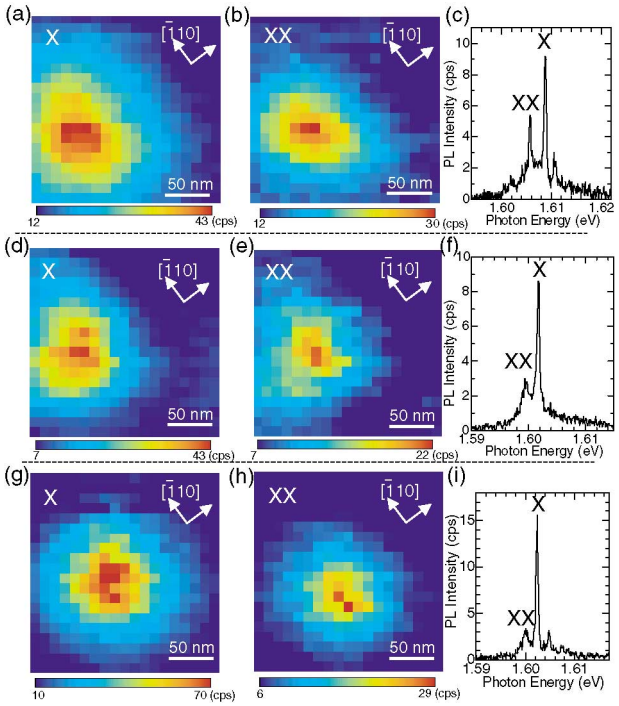


FIG. 3 (color). (a)–(i) Series of high-resolution PL images of exciton state [(a), (d), and (g)], biexciton state [(b), (e), and (h)], and corresponding PL spectra [(c), (f), and (i)] for three different QDs. Scanning area is $210 \times 210$ nm$^2$. Crystal axes along [110] and [$\bar{1}$10] directions are indicated. PL image sizes of biexciton are always smaller than those of exciton.

low-magnification PL maps for the intensity of X emissions with three different energies in the same scanning area. These exciton PL maps show emission profiles of individual QDs, which are seen as bright and individual spots.

The high-magnification PL images in Fig. 3 were obtained by mapping the PL intensity with respect to the X [3(a), 3(d), and 3(g)] and the XX [3(b), 3(e), and 3(h)] lines of three different QDs. The exciton PL images in Figs. 3(a), 3(d), and 3(g) show an elongation along the [$\bar{1}$10] crystal axis. The image sizes are larger than the PL collection spot diameter, i.e., the spatial resolution of the NSOM [23]. The elongation along the [$\bar{1}$10] axis due to the anisotropy of the monolayer-high island is consistent with previous observations with a scanning tunneling microscope (STM) [5]. We also obtained elongated biexciton PL images along the [$\bar{1}$10] crystal axis in

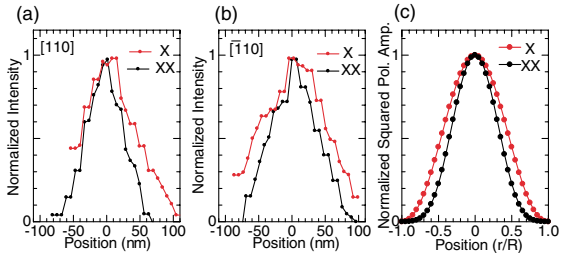


FIG. 4 (color). (a),(b) Normalized cross-sectional intensity profiles of exciton (red) and biexciton (black) PL images corresponding to Figs. 3(a) and 3(b). (c) Normalized spatial distribution of squared polarization fields of the exciton (red) and biexciton (black) emission, which are theoretically calculated for a GaAs quantum disk (radius of 114 nm and thickness of 5 nm). The horizontal axis is normalized by the disk radius $R$.

Figs. 3(b), 3(e), and 3(h) and found a clear difference in the spatial distribution between the exciton and biexciton emission. Here the significant point is that the PL image sizes of biexcitons are always smaller than those of excitons, which will be discussed below. Figures 4(a) and 4(b) show the normalized cross-sectional PL intensity profiles of exciton (red) and biexciton (black) [corresponding to the profile of Figs. 3(a) and 3(b)] along the [110] and [$\bar{1}$10] crystal axes. The spreads in the exciton (biexciton) images, defined as the full width at half maximum (FWHM) of each profile are 80 (60) nm and 115 (80) nm along the [110] and [$\bar{1}$10] crystal axes, respectively.

Theoretical considerations can clarify what we see in the exciton and biexciton PL images. The relevant quantity is the optical near field around a single QD associated with an optical transition. This field can be calculated with Maxwell's equations using the polarization field of the exciton or biexciton as the source term. The observed luminescence intensity is proportional to the square of the near field detected by the probe. In the following, however, we have calculated the emission patterns simply by the squared polarization fields without taking account of the instrumental details, because the obtained PL spatial profiles are much larger than the spatial resolution of 30 nm. The polarization fields are derived from the transition matrix element from the exciton state (X) to the ground state (0) and that from the biexciton state (XX) to the exciton state (X) as follows [26]:

$$\langle 0|p\delta(r-r_s)|\mathrm{X}\rangle = -2^{1/2} p_{cv} \phi(r_s,r_s), \tag{1}$$

$$\langle \mathrm{X}|p\delta(r-r_s)|\mathrm{XX}\rangle = -(3/2)^{1/2} p_{cv} \sum_{r_1,r_a} \phi(r_1,r_a)\Phi^{++}(r_1,r_s;r_a,r_s) - (1/6)^{1/2} p_{cv} \sum_{r_1,r_a} \phi(r_1,r_a)\Phi^{--}(r_1,r_s;r_a,r_s), \tag{2}$$

where $\phi(r_e, r_h)$ stands for the exciton envelope function with the electron and hole coordinates denoted by $r_e$, $r_h$, $\Phi^{++}(\Phi^{--})(r_1, r_2; r_a, r_b)$ represents the biexciton envelope function with electron coordinates $(r_1, r_2)$ and hole coordinates $(r_a, r_b)$ that is symmetrized (antisymmetrized) with respect to the interchange between two electrons and between two holes, and $p_{cv}$ is the transition dipole moment between the conduction band and the valence band at the $\Gamma$ point. As seen in Eq. (1), the spatial distribution of the exciton polarization field corresponds to the center-of-mass envelope function of a confined

exciton. For the biexciton emission, the polarization field is determined by the overlap integral between the radiative recombination amplitude of one of the two electron-hole pairs forming the biexciton and the exciton envelope function of the final state. If $\Phi^{++}$ ($\Phi^{--}$) can be given by a simple product of two exciton envelope functions, i.e., there is no correlation between two excitons, it can be shown that Eq. (2) is proportional to $\phi(r_s, r_s)$ and the spatial profile is the same for both the exciton and the biexciton emissions. However, since the biexciton state is a bound state, the actual $\Phi^{++}$ ($\Phi^{--}$) is spatially more localized compared to the simple product of two exciton envelope functions. Thus the overlap integral in Eq. (2) is more localized than $\phi(r_s, r_s)$, reflecting the spatial correlation between two excitons forming the biexciton.

The squared polarization amplitudes of the exciton and biexciton emission have been calculated for a GaAs quantum disk with size parameters relevant to our experiments (disk radius of 114 nm and thickness of 5 nm). Because of the weak confinement in the lateral direction, the exciton envelope function can be approximated by the two-dimensional hydrogenic bound state for the electron-hole relative motion multiplied by the weakly confined center-of-mass wave function. In the same way, the biexciton envelope function can be approximated by the product of the biexciton wave function in QW [27] for the four-particle relative motion and the confined center-of-mass wave function in the lateral direction. As shown in Fig. 4(c), the calculated profile of the squared polarization amplitude of the biexciton emission (black line) is narrower than that of the exciton emission (red line). The spread of the biexciton emission normalized by that of the exciton emission [defined by the ratio of FWHM of calculated profiles in Fig. 4(c)] is estimated to be 0.76, which is in good agreement with the experimental result ($0.72 \pm 0.08$). This theoretical support and the experimental facts (PL image sizes larger than the spatial resolution, and the optical image of the elongated shape reflecting the anisotropy of a monolayer-high island) lead to the conclusion that the local optical probing by the near-field scanning optical microscope directly maps out the center-of-mass wave function of an exciton confined in a monolayer-high island.

The success of the real-space mapping of the exciton wave function described above is a step toward the realization of quantum devices, because the combination of local optical probing with time-domain coherent control using ultrafast laser pulses will permit advanced manipulation of the QD wave function with direct monitoring of the shape and extent of the wave function itself. Moreover, the optical probe, with its high spatial precision of 30 nm, provides a bridge between the measurements of nanometer-resolution electron microscopy and wavelength-resolution far-field optical spectroscopy, and can play an active role in the characterization of not only well-defined systems as demonstrated here, but also unknown material systems in diverse fields of research.

We thank M. Ohtsu and S. Mononobe for technical advice including the fabrication of optical fiber probe. A part of this work by K. M. and T. T. is supported by the Grant-in-Aid for Scientific Research from JSPS (Japan Society for the Promotion of Science). A part of this study was supported by CREST, JST. This study was supported in part by the Active Nano-Characterization and Technology Project, Special Coordination Funds of the Ministry of Education, Culture, Sports, Science and Technology of the Japanese Government.

*Electronic address: matsuda@net.ksp.or.jp

[1] A. Imamoglu *et al.*, Phys. Rev. Lett. **83**, 4204 (1999).
[2] A. Zrenner *et al.*, Nature (London) **418**, 612 (2002).
[3] Z. Yuan *et al.*, Science **295**, 102 (2002).
[4] K. Brunner *et al.*, Phys. Rev. Lett. **73**, 1138 (1994).
[5] D. Gammon *et al.*, Phys. Rev. Lett. **76**, 3005 (1996).
[6] M. Bayer *et al.*, Nature (London) **405**, 923 (2000).
[7] M. Bayer *et al.*, Science **291**, 451 (2001).
[8] L. Landin *et al.*, Science **280**, 262 (1998).
[9] G. Chen *et al.*, Phys. Rev. Lett. **88**, 117901 (2002).
[10] T. H. Stievater *et al.*, Phys. Rev. Lett. **87**, 133603 (2001).
[11] N. H. Bonadeo *et al.*, Science **282**, 1473 (1998).
[12] J. R. Guest *et al.*, Phys. Rev. B **65**, 241310 (2002).
[13] J. R. Guest *et al.*, Science **293**, 2224 (2001).
[14] Q. Wu *et al.*, Phys. Rev. B **62**, 13 022 (2000).
[15] C. Chicanne *et al.*, Phys. Rev. Lett. **88**, 097402 (2002).
[16] A. Dereux, C. Girard, and J. Weeber, J. Chem. Phys. **112**, 7775 (2000).
[17] G. W. Bryant, Appl. Phys. Lett. **72**, 768 (1998).
[18] C. D. Simserides *et al.*, Phys. Rev. B **62**, 13 657 (2000).
[19] H. F. Hess *et al.*, Science **264**, 1740 (1994).
[20] S-K. Eah, W. Jhe, and Y. Arakawa, Appl. Phys. Lett. **80**, 2779 (2002).
[21] F. Intonti *et al.*, Phys. Rev. Lett. **87**, 076801 (2001).
[22] K. Matsuda *et al.*, Appl. Phys. Lett. **76**, 73 (2000).
[23] K. Matsuda *et al.*, Appl. Phys. Lett. **81**, 2291 (2002).
[24] T. Saiki and K. Matsuda, Appl. Phys. Lett. **74**, 2773 (1999).
[25] In Fig. 2(a), broad background PL due to the electron-hole plasma superimposes on the PL spectra [14]. The PL intensities of the X and XX lines were estimated by fitting the background by Lorentzian function and subtracting it from the PL spectrum.
[26] S. V. Nair and T. Takagahara, Phys. Rev. B **55**, 5153 (1997).
[27] D. A. Kleinman, Phys. Rev. B **28**, 871 (1983).